WILEY | Hindawi

Research Article

Optimization and Practice for Partition Pressure Relief of Deep Mining Roadway Using Empty-Hole and Deep-Hole Blasting to Weaken Coal

Baobao Chen [iD],[1] **Changyou Liu** [iD],[2] and **Fengfeng Wu** [iD][2]

[1]*State Key Laboratory of Mining Response and Disaster Prevention and Control in Deep Coal Mines, Anhui University of Science and Technology, Huainan 232001, China*
[2]*State Key Laboratory of Coal Resources and Safe Mining, China University of Mining and Technology, Xuzhou 221116, China*

Correspondence should be addressed to Changyou Liu; lcycumt@cumt.edu.cn and Fengfeng Wu; miningcumt@163.com

Rockbursts are among the most harmful dynamic disasters, threatening the personnel safety and mine operation. In order to alleviate stress concentration of roadsides and prevent rockbursts, the large-diameter boreholes and deep-hole blasting are employed for partition pressure relief in the deep mining roadway. Combined with failure behavior and stress distribution of the coal, the multilevel division of risk degree for roadsides stress is determined. Based on the orthogonal test of borehole pressure relief in the general danger partition, the response degree of quantitative indexes to main factors influencing the pressure relief effect is considered. The optimal drilling parameters of 120.0 mm diameter, 20.0 m depth, 1.0 m hole spacing, and 5° elevation angle are obtained, determining the stress boundary of safe pressure relief with boreholes. At higher dangerous stress divisions, the optimized blasting parameters through numerical simulation could be obtained as follows: 15.0 m depth, 1.3 decoupling coefficient, and 2.0 m hole spacing, and meanwhile, a stress relief partition of crisscross cracks with 0.61 m height is formed. The roadsides stress could be well controlled within the safe level. Then, an optimal combination of pressure relief is applied to different stress partition of roadsides, and the effectiveness is validated by field test, which proves remarkably applicable for engineering.

1. Introduction

With the increasing depth of coal mining, the self-weight stress of original rock is increasing significantly [1, 2]. In addition, the stress concentration induced by the geological structure and mining would lead to the stress peak of roadsides exceeding the coal strength [3]. High stress concentration of surrounding rock is responsible for large deformation of roadsides, rockbursts, and so on, which poses more serious threat to efficient production and personal safety. Therefore, it is necessary to strengthen the research and application of pressure relief, achieving safe mining. Only when the active measures of weakening coal are adopted could stress transfer be achieved to reduce the potential risk of dynamic instability [4, 5].

Comparatively speaking, the active pressure relief measures for the coal are usually based on enlarging migration space and weakening the coal strength, mainly including the large-diameter boreholes, deep-hole presplitting blasting, water-infusion softening, and roadway (chamber) excavation in the coal [6–8]. The application of water-infusion softening coal has higher requirements for the geological condition and process and hardly to achieve significant effect of pressure relief in a short time [9]. Meanwhile, the chamber (pressure relief roadway) excavation needs relatively high economic cost with long operating periods and results in the large coal pillar loss. However, due to strong adaptability for geological conditions, low cost, and simple technology, the large-diameter boreholes and deep-hole presplitting blasting as the regional pressure relief of roadsides

coal are widely used in the stress transfer of the deep coal, which achieve good technical effects in the multiple stress environments and improve the mining safety. Scholars at home and abroad have done lots of research on the stress transfer mechanism and evaluated the controlling effect of pressure relief. The mechanism of borehole pressure relief was analysed and the main controlling parameters on pressure relief effect was determined, proposing the evaluation indexes and degree classification of stress relief effect [10]. Based on failure characteristics of the coal, the migration characteristics of fracturing coal and the pressure relief rationality of the large-diameter boreholes were illustrated [11]. The response of coal stress relief effect to mechanical parameters and the safety degree were analysed, obtaining the applicable conditions [12]. FRACOD software was used for simulating the initiation and propagation of cracks around the boreholes, and the pressure relief effect of different types of boreholes is analysed. A new method for selecting the optimal technical parameters of pressure relief boreholes was proposed [13]. However, the application of large diameter boreholes in stress relief is limited to a certain stress range, which could achieve good effect. When the regional stress reaches a certain degree, the further increase of borehole diameter and length as well as the decrease of hole spacing has no significant effect on promoting pressure relief effect. On the contrary, it is not conducive to the maintenance of the mining roadway [14]. Meanwhile, the roadsides coal after pressure relief still has the impact risk. Therefore, after the stress exceeds the critical value, the deep-hole blasting is employed for improving the coal fracturing characteristics and further enlarging the cavity, to strengthen the pressure relief effect. In terms of blasting stress relief, the deep-hole blasting was adopted at different advance of working face, which ensured the panel to be safely extracted without any rockbursts [15]. To improve effectiveness of blasting distressing, the research focused on the multiaxis stress evolution as well as the optimized utilization of blasting energy on the initiation and propagation of cracks [16]. Due to the multifactors acting on the stress relieving effect, it was necessary to replace the traditional variable method with orthogonal test [17]. Considering limitation of the field application, the selection of optimal technical scheme was determined by the combination of numerical simulation and theoretical analysis.

The above research mainly adheres to the analysis on the pressure relief parameters and stress controlling effect under the specific stress boundary and lacks pressure relief simulation of multilevel dangerous partition of high stress concentration induced by complicated original rock stress. Consequently, based on the diversity of geological conditions of the working face in Gucheng mine, the piecewise distribution characteristics of in situ stress and the risk degree of high stress concentration are obtained. Combined with main technological parameters of influencing pressure relief effect and quantitative indexes of stress-transfer degree, an orthogonal test adopts LS-DYNA simulation to achieve optimal parameter combination and the application range of safety pressure relief. After exceeding the critical stress, the simulation of distress blasting is employed for elaborating the characteristics of enlarging cavity and presplitting coal to obtain the stress transfer effect between blasting holes. The stress relief parameters are applied on site to verify the effectiveness of partition pressure relief via monitoring abutment stress and deformation of roadsides.

2. Risk Level Evaluation of High Stress and Stress Transfer Mechanism of Weakening Coal

2.1. Mining Technical Conditions of Working Face. 3# coal, as the main coal seam in Gucheng coal mine, has an average dip angle of 5° and thickness of 8.6 m. The absolute gas emission is 0.06 m³/min (the relative gas emission is 0.02 m³/t), and it is determined as a low gas mine with the low risk of coal and gas outburst. The fully mechanized caving face has a length of 120.0 m with an average depth of 1100.0 m. The coal seam has the strong impact tendency, and the strata distribution is shown in Figure 1. The mining roadways are constructed along the floor and adopt bolt-mesh-anchor support. The section has a shape of straight wall with semicircle arch, with the net width of 5.2 m and the straight wall height of 1.8 m. According to the three-dimensional seismic exploration, it is estimated that 3 large faults would be exposed during the excavation, as shown in Figure 2.

In order to reduce the dynamic disaster induced by mining stress concentration, the method of drilling pressure relief prior to excavation in the mining roadway is adopted. There are three boreholes in the head-on, in which one is in the middle, and each one for both sides has a horizontal angle of 45°. The drilling hole spacing is 1.0 m, and the diameter is 110.0 mm. The boreholes are arranged 0.7 m away from the floor with the depth no less than 20.0 m. The horizontal elevation of the borehole is 5°, and the boreholes are drilled every 10.0 m of excavation. The parameter arrangement of drilling pressure relief is shown in Figure 3. Heading pressure relief during excavation reduces gas content and pressure, which could effectively reduce the occurrence of gas outburst caused by deep-hole blasting.

2.2. Multifactor Coupling Analysis on Original Rock Stress Partition. During the excavation of the deep mining roadway, the pressure gradually transferring to the deep coal results in stress concentration of roadsides, which increases the possibility of coal dynamic disaster. In particular, when the roadside is within the influence range of fault tectonic stress, the stress concentration makes it easy to accumulate more energy. The stress concentration factor and influence range are shown in Table 1. In order to quantitatively describe the stress distribution characteristics on both sides of faults, it is simplified as an isosceles triangle [3], as shown in Figure 4.

The intersection point of mining roadway and open cutting in 3200 working face is taken as the coordinate origin. According to the change trend of the buried depth (Figure 2), the roadway is approximately divided into 5

Lithologic characters	Legend	Thickness	Description of lithologic characteristics
Argillaceous sandstone		4.50	Dark gray brittle sandstone with block structure. Fissure, filling calcite veins and local silt band
Silty sandstone		5.70	Dark gray with block structure, containing carbonaceous and sandy mudstone
Fine sandstone		4.75	Quartz-based and hard argillaceous cementation, with carbon surfaces
Medium sandstone		18.70	Quartz-based, containing intermittent horizontal bedding and calcareous sandstone in the bottom
Sandy mudstone		1.88	Gray brittle mudstone with block structure, containing fossil plants and sliding surface
3# coal		8.60	Semi-bright black bituminous coal containing specular coal strip, with banded structure
Sandy mudstone		2.28	Black mudstone with carbon-entrapped, and flake minerals along the horizon
Medium sandstone		3.00	Hard medium sandstone with slime calcareous cementation and wavy bedding
Sandy mudstone		2.30	Black-grey, filling the fine sandstone bands and horizontal bedding

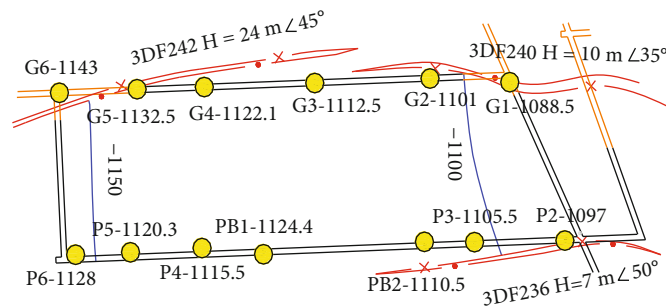Figure 1: Strata distribution of 3# coal roof and floor.

Figure 2: Geological condition of 3200 working face. Note: *P* represents the exploration point along the conveyor entry; *G* represents the exploration point along the tail entry.
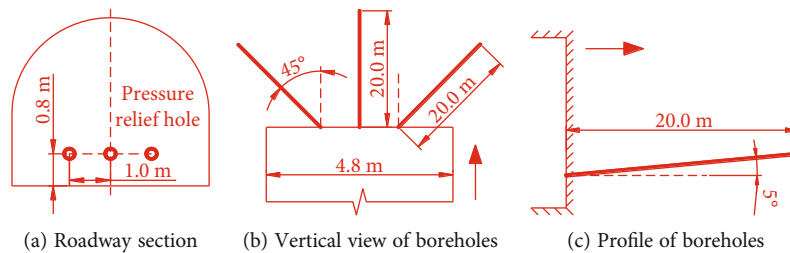

(a) Roadway section   (b) Vertical view of boreholes   (c) Profile of boreholes

Figure 3: Design parameter of pressure relief drilling in the heading face.

TABLE 1: Fault parameters of 3200 working face.

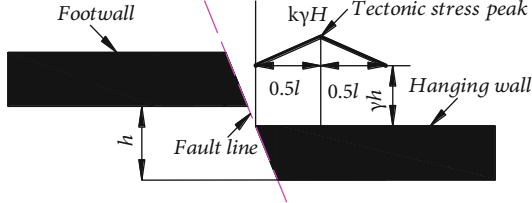| Fault name	Drop (m)	Stress concentration factor	Distance from fault (m)	Unilateral influence range (m)
DF242	24	1.4	43	80
DF240	10	1.3	15	60
DF236	7	1.3	38	60

FIGURE 4: Tectonic stress distribution of fault. Note: γH is the in situ stress of the coal mass; k is the tectonic stress concentration factor under the influence of the fault; l is the unilateral influence range of the fault; h is fault drop.

FIGURE 5: Stress distribution curve of the roadsides.

segments and 6 nodes, and the distribution curve of self-weight stress is shown in Figure 5.

Taking the tail entry as an example, in combination with Table 1, the coal stress near the coordinate origin is basically not affected by the fault 3DF242 (0-93.0 m) and determined as self-weight stress. Within 93.0-418.7 m, the distance between fault and the mining roadway increases approximately linearly, and the maximum stress concentration factor is 1.15. Within 418.7-448.0 m, under the influence of the superimposed tectonic stress of fault 3DF242 and 3DF240, the regional stress concentration factor is set to be 1.4. Within 448.0-660.0 m, the distance between the roadsides and the fault is just 1/4 of the influence range, and the stress concentration factor is determined as 1/2 of the maximum value, i.e., 1.15. According to the parameter variation of 3DF236 fault, the three-section distribution characteristic function of the in situ stress of the conveyor entry is also obtained. The piecewise function employed for illustrating the distribution of σ_{gg} (in situ stress of tail entry) and σ_{gp} (in situ stress of conveyor entry) is shown in

$$
\begin{cases}
\sigma_{gg} = \begin{cases}
1.15\sigma_g & (448, 660), \\
1.4\sigma_g & (418.7, 448), \\
\sigma_g + \dfrac{0.15\sigma_g}{325.7}(x - 93) & (93, 418.7), \\
\sigma_g & (0, 93),
\end{cases} \\[2em]
\sigma_{gp} = \begin{cases}
\sigma_p + \left[0.3\sigma_p - \dfrac{0.3\sigma_p}{244}(x - 508)\right] & (508, 752), \\
1.3\sigma_p & (440, 508), \\
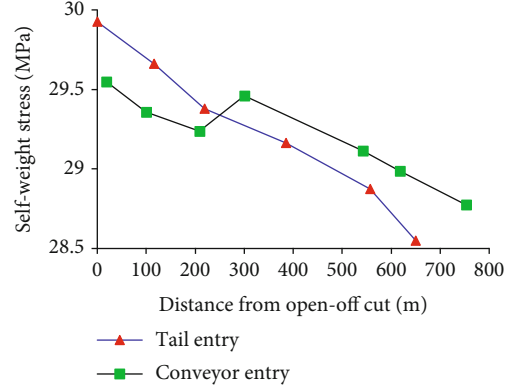\sigma_p & (0, 440).
\end{cases}
\end{cases}
\tag{1}
$$

Note: σ_g and σ_p are self-weight stress of tail and conveyor entry, respectively.

When the coal stress is more than $1.5\sigma_c$ (σ_c: uniaxial compressive strength, 19.2 MPa), the dynamic disaster is easy to occur [18, 19]. Therefore, the demarcation stress value for the general-, medium-, and high-risk region is set to be $1.5\sigma_c$, $1.8\sigma_c$, and $2.0\sigma_c$, respectively, shown in Table 2. Combining with Equation (1), the contour diagram of roadside stress distribution is obtained by the linear interpolation. The three danger partitions are 28.8-34.56 MPa (G), 34.56-38.4 MPa (M), and more than 38.4 MPa (H), as shown in Figure 6. When the roadsides stress is higher than the general danger line, the active stress relief measures should be adopted in time during the excavation.

2.3. Pressure Relief Mechanism of Fracturing Coal and Applicability of the Measures.

In order to ensure the safe excavation of high stress roadway, the corresponding measures for stress relieving are adopted combined with the partition of roadsides stress. On the basis of the stress transfer (Figure 7) in stress relief zone, the large-diameter boreholes and deep-hole blasting are employed for fracturing coal to accomplish partition pressure relief.

When the active measures are employed for destroying the coal structure, the coal mass would be damaged to form a weakening zone, which leads to the significant decrease in the roadside stress and the slope of postpeak stress curve (avoiding stress mutation). The stress would be transferred to the deep obviously and the plastic zone continues to expand, which reduce the elastic energy accumulation of the coal to the safe level. Meanwhile, the pressure relief coal near roadsides produces a low stress protection zone ("wedge-shaped" resistance bands) with large width and low density of coal. Safety strategy of partition pressure relief

TABLE 2: Division of stress segment and risk.

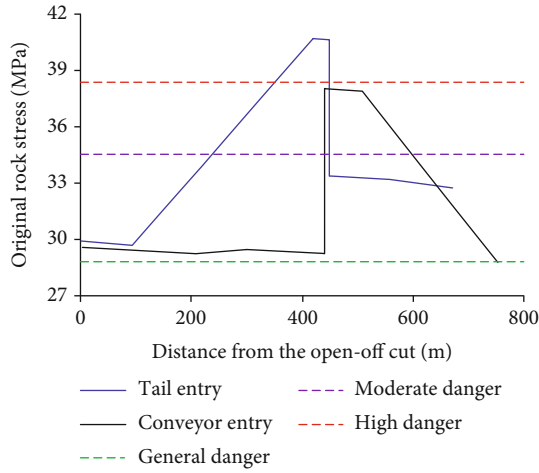| Name Region (S)	Critical value		Stress relief None
General-risk region (G)	$1.5\sigma_c$	28.8 MPa	Stress relief
Medium-risk region (M)	$1.8\sigma_c$	34.56 MPa	Stress relief
High-risk region (H)	$2.0\sigma_c$	38.4 MPa	Stress relief

FIGURE 6: Stress distribution contour diagram of roadsides. Note: the green line is G region; the purple line is M region; the red line is H region.

plays the role of releasing dynamic loading and buffering the rockbursts, thereby reducing the impact risk of coal [20].

The coal with drilling large-diameter boreholes would be fractured under the action of high stress, to form a fracture zone much larger than the borehole diameter. Then, the fracturing zones would be cross-connected with each other to induce a larger range of pressure relief zone. The continuous extension of the pressure relief range leads to the stress concentration zone near roadsides transferred to the deep as a whole. The borehole diameter and hole spacing determine the stress transferring degree of the coal between boreholes. On this basis, the transfer depth of peak stress depends on the drilling depth to a certain extent. With the strengthening of pressure relief parameters (hole spacing decreasing and the diameter and depth of boreholes increasing), the stress concentration zone continues to transfer to the depth of the coal and the pressure relief effect is enhanced.

The pressure relief of the deep-hole presplitting blasting is the concentrated charging blasting at the bottom of the drilling borehole to separate the blasting coal from the deep coal. Blasting not only releases the elastic energy accumulated in the coal but also could produce a loosening zone to absorb the impact and deformation of the coal, so as to alleviate the stress concentration near the roadsides. The reasonable blasting parameters could promote the degree and range of coal fracturing and strengthen the pressure relief degree and peak transfer depth, which is suitable for a wide range of stress boundary.

The pressure relief measures are suitable for various stress conditions due to different action mechanisms, but also have limitations. Borehole pressure relief could provide effective compensation space for coal expansion and absorb partial deformation during stress transfer. However, the higher mining stress is conducive to the fracturing of the drilled coal to induce pressure relief, but the efficiency decreases significantly. At the moment, the pressure relief effect is not significantly improved by increasing the hole diameter and reducing the hole spacing. The stress transfer caused by coal drilling cracks shows the characteristics of slow growth, and pressure relief shows obvious lagging in drilling. Meanwhile, the roadside coal is affected by borehole collapse, which would influence the local support structure. Deep-hole blasting is suitable for pressure relief in complex stress environment. The increase of presplitting strength promotes the migration range and degree of the fracturing coal. However, during excavation of the mining roadway, the interference between excavation and pressure relief implementation reduces the roadway forming speed. Deep-hole blasting may cause vibration damage of the roadsides coal and aggravate coal deformation, which increases the difficulty of roadway support. Therefore, the attention should be paid to the length and strength of hole sealing and the charging position, in order to reduce the damage of blasting to coal.

Therefore, the limitations of pressure relief technology should be reasonably utilized and avoided to improve the pressure relief efficiency in the field production.

3. Feasibility of Safe Strategy on the Pressure Relief of Large-Diameter Borehole Based on the Orthogonal Test

3.1. Design of Orthogonal Test Scheme. Under the condition of the lower roadside pressure (G), large-diameter boreholes are proposed for pressure relief. Orthogonal simulation test is employed for optimizing drilling parameters, and the selection of influencing factors and levels is shown in Table 3. The measurement factor of pressure relief degree adopts significant indexes $I1$ and $I2$ as well as an auxiliary index $I3$. $I1$ and $I2$ reflect the stress transfer degree of the roadside coal, while $I3$ could indirectly reflect the migration degree of the fracturing coal. After stress reaches a safe level, the deformation should be comprehensively considered to avoid the greater difficulty of roadway support.

Typically, the orthogonal test with four factors and three levels requires fewer than 12 tests. Considering that numerical simulation is convenient and could be performed at a competitive price, the test adopts the orthogonal test design L16 (3^5) without reiteration, in which the last column is regarded as an error.

The numerical model of pressure relief near roadsides is established using ANSYS, in which physical-mechanical parameters are shown in Table 4.

Considering the influence of boundary stress concentration, the model has dimensions of 65.2 m × 15.0 m × 36.2 m. Pressure relief holes are arranged perpendicularly into a

(a) Drilling

(b) Deep-hole presplitting blasting
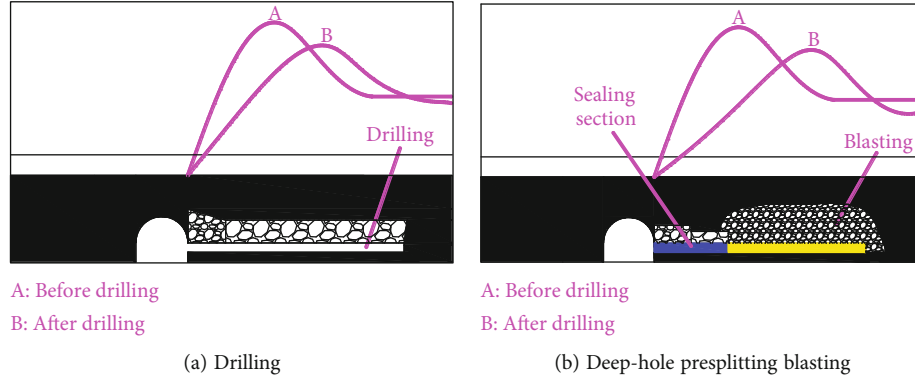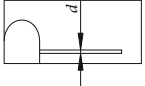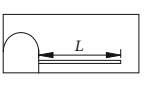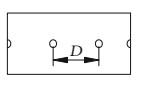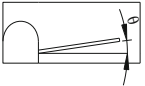
FIGURE 7: Stress transfer of weakening coal mass in roadsides.

TABLE 3: Multifactor and indexes of orthogonal simulation test.

Pressure relief parameter				Index (I)
A (mm)	B (m)	C (m)	D (°)	
Diameter	Length	Spacing	Elevation angle	
90, 100, 110, 120	12, 15, 18, 20	1, 2, 3, 4	0, 5, 10, 15	(1) Peak stress position (I1); (2) stress in the near field (I2); (3) deformation of roadsides (I3)

Note: based on the theoretical calculation of the abutment pressure of the roadsides without pressure relief, it is obtained that the peak stress is at 6.5 m from the roadsides; therefore, the stress at 6.5 m is determined as I2.

TABLE 4: Physical-mechanical parameters.

Lithology	Density (kg/m^3)	Elastic modulus (GPa)	Poisson's ratio	Internal friction angle (°)	Cohesion (MPa)
Fine sandstone	2600	38.8	0.22	33.2	11.7
Medium sand	2650	63.2	0.18	36.2	28.0
Mudstone	2500	18.9	0.28	43.2	9.7
Coal	1400	6.7	0.22	25.2	6.8

single row in the roadsides, as shown in Figure 8. The model boundary restricts the horizontal displacement and velocity, while the bottom controls vertical component. A vertical load of 28.8 MPa is applied for the upper boundary of the model.

3.2. Simulation Result Analysis of Pressure Relief Effect. Through the orthogonal test, the position of abutment pressure peak and stress in 6.5 m from roadsides and the roadway deformation are obtained. The orthogonal test data is illustrated, as shown in Table 5, where KL_i ($i = 1, 2, 3, 4$) is the average index value under different factors, while the curves indicate the response degree of the inspection indexes to various factors.

Based on the extreme value variation, the rational order of multifactors on I1 is A-B-C-D-E, with the optimal combination is A4B4C2D4, namely, 120.0 mm diameter, 20.0 m depth, 2.0 m hole spacing, and 15° elevation angle. For I2,

the optimal combination is determined with A4C1B2D4, meaning 120.0 mm diameter, 1.0 m hole spacing, 15.0 m depth, and 15° elevation angle. Considering I3, the combination is A1C4D2B3, meaning 90.0 mm diameter, 4.0 m hole spacing, 5° elevation angle, and 18.0 m depth.

In the orthogonal test, the significance level is an important parameter to evaluate the influence of factors. When the factors do not obey the Gaussian distribution, it is unreasonable to only implement the variance analysis. The significance and contribution rate are employed for determining the optimized parameters, which are corresponding to extreme value analysis, but more accurate. The greater the contribution rate is, the more important it is. When contribution rate of some factors is similar to that of the error, the level of factors should be selected according to field conditions [21]. The significance and contribution rate of the four factors on three indexes are shown in Tables 6 and 7.
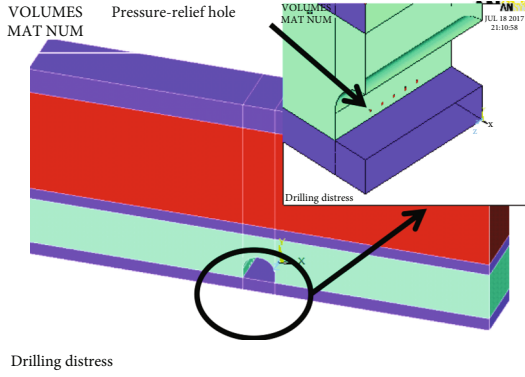
FIGURE 8: Simulation model of deep-hole blasting pressure relief.

For $I1$, due to F_A, F_B, and F_C are greater than $F_{0.05}(3, 15) = 3.29$, the factors A, B, and C are significant at the level of 0.05 while factor D is opposite. Based on the contribution rate of factor B slightly larger than that of error, the optimal combination is $A4BC2D$ (the alternative scheme is $A4B4C2D$). Aiming at $I2$, F_A and F_C are greater than $F_{0.05}(3, 15) = 3.29$, that is, factors A and C are significant at the level of 0.05. Therefore, the optimal combination is $A4BC1D$. For the auxiliary index $I3$, F_A and F_C are greater than $F_{0.05}(3, 15) = 3.29$, that is, factors A and C are significant at the level of 0.05. The combination of optimal factors is $A1BC4D$. In the orthogonal test, the parameters of 15 and 16 schemes could achieve significant effect of pressure relief, meeting the safety requirements. Combined with the significant indexes, the optimal combination could be set with $A4B4C1D$ or $A4B4C2D$. Since the elevation angle is a nonsignificant factor, considering the site construction, the elevation angle of boreholes is set to be 5°, which is not only convenient for construction but also conducive to release of the drilling dust. Therefore, the final scheme is determined to be $A4B4C1D2$, namely, 120.0 mm diameter, 20.0 m depth, 1.0 m hole spacing, and 5° elevation angle.

According to the above, the optimal parameters of pressure relief are obtained under the condition of 28.8 MPa boundary stress. Under the optimal parameters, the response of the three indexes ($I1$, $I2$, and $I3$) to the variation of boundary stress is shown in Figure 9.

With the increase of boundary stress, the transfer depth of stress peak after pressure relief decreases slowly, and meanwhile, the stress peak increases approximately linearly. Under the upper boundary value (34.56 MPa) of medium dangerous stress range, the transfer depth and value of stress peak are, respectively, 4.42 m and 28.7 MPa, showing that the stress peak is transferred into the deep and the roadsides stress has dropped to the safe level. The above reveals the borehole pressure relief with the optimal parameters could achieve good stress controlling effect (less than 28.8 MPa) and promote the safety production degree of working face. However, the pressure relief parameters of large-diameter borehole are unable to achieve the effective effect at the stress partition above

medium risk critical stress (34.56 MPa). With the increase of the diameter and the decrease of the hole spacing, the strengthening effect of pressure relief is not significantly improved and the drilling workload increases exponentially. Therefore, another safety strategy, deep-hole presplitting blasting with noncoupling charge, is proposed for pressure relief in partition S and M.

4. Safety and Applicability of Pressure Relief Effect with Deep-Hole Blasting in Higher Stress Risk Region

Because the large-diameter hole provides limited radial compensation space for coal transfer, stress relief effect can only be achieved within local range. Meanwhile, the possibility of coal and gas outburst in low gas mines is small, and deep-hole blasting could be applied. Deep-hole presplitting blasting will further strengthen the coal fracturing density and weakening range, as well as promote the safety degree of pressure relief.

4.1. Theoretical Analysis of Blasting Parameters for Weakening Coal. The main basis for measuring the blasting effect is the range of the crushing and initial fracturing zone caused by stress wave. Based on cylindrical explosive charge and stress attenuation coefficient, the destroying radius is

$$\begin{cases} P_m = \dfrac{\rho_0 D^2 n}{8} \left(\dfrac{r_c}{r_b}\right)^{-6}, \\[2mm] R_c = \left[P_m \cdot \dfrac{B}{\sqrt{2}\sigma_{cd}}\right]^{1/\alpha} \cdot r_c, \\[2mm] R_P = \left(\dfrac{\sqrt{2}\sigma_{cd}}{B\sigma_{td}}\right)^{1/\beta} \cdot R_c, \end{cases} \qquad (2)$$

where P_m is the peak value of transmitted shock wave in the coal mass, R_c is the crushing radius, R_p is the radius of the fracturing zone, ρ_0 is explosive density, D is the detonation velocity, n is the blasting pressurization coefficient, 10, r_c and r_b are the radius of the blast hole and charge, respectively, B is the blasting stress intensity factor, σ_{cd} is the uniaxial dynamic compressive strength, α and β are the attenuation coefficient of shock wave and stress wave, respectively, and σ_{td} is the dynamic tensile strength. The radius of crushing zone and cracks is calculated as 0.12 m and 0.85 m, respectively.

The crack field is caused by the interaction of blasting stress wave and detonation gas. The action of detonation gas is a quasistatic process and acts on the tip of cracks together with the in situ stress. When the static fracture criterion is met, the coal at tensile yield induces the secondary continuous expansion of cracks [22]. Assuming that the pressure of explosion gas $p(r)$ is uniformly distributed along the initial crack surface and the selected value of in situ stress σ_h is 40.5 MPa, then the stress distribution from the hole

TABLE 5: Statistical analysis of orthogonal test results.

No.	Factor					I1 (m)	I2 (MPa)	I3 (mm)
	A	B	C	D	Error			
1	90	12	1	0	1	9.02	29.93	157.59
2	90	15	2	5	2	9.70	30.71	152.68
3	90	18	3	10	3	9.40	32.38	149.35
4	90	20	4	15	4	9.70	32.20	149.12
5	100	12	2	15	3	10.41	29.84	165.72
6	100	15	1	10	4	10.51	28.18	168.36
7	100	18	4	5	1	9.59	31.50	157.59
8	100	20	3	0	2	9.81	30.10	160.12
9	110	12	3	5	4	9.39	27.91	168.20
10	110	15	4	0	3	10.21	28.26	165.98
11	110	18	1	15	2	10.91	25.90	176.14
12	110	20	2	10	1	11.32	26.51	171.69
13	120	12	4	10	2	10.00	27.65	178.15
14	120	15	3	15	1	11.00	25.55	179.32
15	120	18	2	0	4	11.21	24.41	183.57
16	120	20	1	5	3	11.79	23.98	187.53
$I1$								
KL_1	9.46	9.71	10.56	10.06	10.23			
KL_2	10.08	10.36	10.66	10.12	10.11			
KL_3	10.46	10.28	9.90	10.31	10.45			
KL_4	11.00	10.66	9.88	10.51	10.20			
Range	1.55	0.95	0.79	0.44	0.35			
$I2$								
KL_1	31.30	28.83	26.99	28.18	28.37			
KL_2	29.90	28.18	27.87	28.53	28.59			
KL_3	27.15	28.55	28.98	28.68	28.61			
KL_4	25.40	28.20	29.90	28.37	28.18			
Range	5.91	0.66	2.91	0.50	0.44			
$I3$								
KL_1	152.19	167.42	172.40	166.82	166.55			
KL_2	162.95	166.59	168.41	166.50	166.77			
KL_3	170.50	166.66	164.25	166.89	167.15			
KL_4	182.14	167.11	162.71	167.58	167.31			
Range	29.96	0.83	9.69	1.08	0.77			
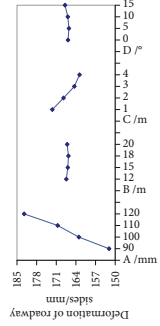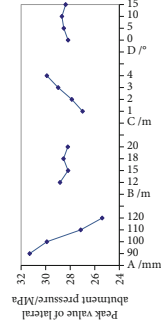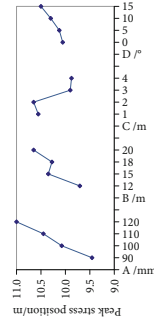
TABLE 6: Variance analysis.

F	DEVSQ			DOF	F			Significance		
	I1	I2	I3	f	I1	I2	I3	I1	I2	I3
SSA/MSA	5.07/1.69	85.08/28.36	1909.60/636.53	3	19.61	167.11	1311.54	*	*	*
SSB/MSB	1.89/0.63	1.18/0.39	1.84/0.61	3	7.32	2.31	1.26	*		
SSC/MSC	2.10/0.70	19.42/6.47	228.58/76.19	3	8.14	38.14	156.99	*	*	*
SSD/MSD	0.48/0.16	0.56/0.19	2.46/0.82	3	1.87	1.09	1.69			
SSE/MSE	0.26/0.09	0.51/0.17	1.46/0.49	3						
SST	9.80	106.74	2143.94	15	$(S1) F_{0.1} = 2.490$; $(S2, S3) F_{0.05} = 3.290$					

Note: SST is the sum of squares of total deviations; SSJ (J: A-D) is the sum of squares of deviations of various factors; SSE is the sum of squares of deviations of test errors; MSJ (J: A-D) is the mean of squares of deviations of various factors; f_j (j: A-E) is the degrees of freedom for various factors; f_T is total degrees of freedom; F: the statistical verification value.

TABLE 7: Contribution rate analysis of multifactors.

	Pure sum of squares			Contribute rate (%)			Selection		
	I1	I2	I3	I1	I2	I3	I1	I2	I3
SSA-$f_A \times$ MSE	4.81	84.57	1908.14	49.04	79.23	89.00	4	4	1
SSA-$f_B \times$ MSE	1.63	0.67	0.38	16.66	0.62	0.02	4		
SSA-$f_C \times$ MSE	1.84	18.91	227.13	18.82	17.72	10.59	2	1	4
SSA-$f_D \times$ MSE	0.23	0.05	1.01	2.30	0.04	0.05			
$f_T \times$ MSE	1.29	2.55	7.28	13.18	2.38	0.34			
SST	9.80	106.74	2143.94					**A4B4C1D2**	

wall to the vicinity of crack tip and critical stress condition of micro crack propagation is

$$
\begin{cases}
\sigma_\theta = \dfrac{a}{r^2}\left[r_0 p_0 + \displaystyle\int_{r_0}^a p(r)dr\right] - \sigma_h\left(1 + \dfrac{a^2}{r^2}\right), \\[2mm]
\sigma_{cl} = \sqrt{\dfrac{\pi}{4a_0}}K_{IC} = \sqrt{\dfrac{\pi}{4a_0}}\cdot \alpha_k \dfrac{P_{\min}}{t_h\sqrt{D_l/2}}.
\end{cases}
\tag{3}
$$

σ_θ is the tangential stress; σ_{cl} is the critical stress for crack propagation; K_{IC} is the static fracture toughness; a is initial crack length; $P_{\min}$ is the first minimum value after the peak of tensile strength by the Brazilian test; α_k is the strength attenuation coefficient, taking the value of 0.8; D_l is the sample diameter; t_h is the sample thickness. The calculated K_{IC} is 1.2 MPa.m$^{0.5}$.

Because the detonation gas is confined, it is regarded as the ideal gas with constant entropy expansion. The tangential displacement is due to the action of detonation gas, and the gas pressure is linearly attenuated [23]. The crack length l_x of detonation gas corresponding to pressure p_x is

$$
\begin{aligned}
p_x &= p_0\left[\frac{r_c + R_c + R_p}{r_c + R_c + R_p + l_x}\right]^r = p_c\left[\frac{p_{av}}{p_c}\right]^{r/k}\left[\frac{\pi r_c^2 + \pi R_c^2}{\pi r_c^2 + \pi R_c^2 + \pi R_p^2}\right]^r \\
&\quad \cdot\left[\frac{r_c + R_c + R_p}{r_c + R_c + R_p + l_x}\right]^r.
\end{aligned}
\tag{4}
$$

Then, the stable length $l_{\max (x)}$ of the second fracture expansion is

$$
\begin{cases}
K_{IC}\sqrt{\dfrac{\pi}{4a_{\max}}} = \dfrac{r_1}{a_{\max}^2}\left[(R_c + r_c)p_{av} + R_p p_0 + \displaystyle\int_{r_1}^{a_{\max}} p_x dx\right] - \sigma_h\left(1 + \dfrac{r_1^2}{a_{\max}^2}\right), \\[2mm]
a_{\max} = r_1 + l_{\max (x)} = R_c + r_c + R_p + l_{\max (x)},
\end{cases}
\tag{5}
$$

where P_{av} is the detonation stability stress, generally 200 MPa. The ultimate length $l_{\max (x)}$ of the second expansion of cracks driven by detonation gas is calculated to be 0.14 m.

Therefore, considering the fracturing superposition coefficient of stress wave ($k = 1.1$), the blast hole spacing $l = 2 \times 1.1 \times (R_c + R_p + l_{\max (x)}) = 2.44$ m.
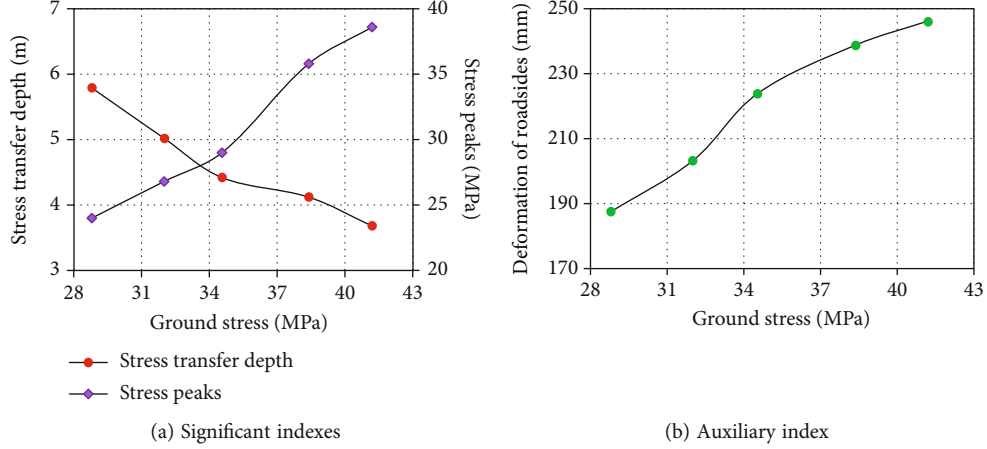
(a) Significant indexes

(b) Auxiliary index

FIGURE 9: Response relation of factors to stress in original rock based on the optimal parameters.

TABLE 8: Explosive parameters.

Density (kg/m^3)	Velocity (m/s)	State equation parameters					
		A (GPa)	B (GPa)	R_1	R_2	ω	E_0 (GPa)
1000	3800	322	3.95	4.15	0.96	0.15	4.192

4.2. Simulation Analysis of Blast-Induced Fracture for Pressure Relief.

The numerical software LS-DYNA^{3D} is applied to establish the model, and ALE is used to calculate the blasting of explosives. The model adopts the nonreflecting boundary condition, and the parameters of emulsion explosive are shown in Table 8 [24]. In order to simulate the coal fracturing, **MAT_ADD_EROSION** is employed for setting failure criterion as shown in Table 9. When one or more conditions are met, the corresponding element will be deleted. The JWL equation (Equation (6)) is adopted to describe the relation between the volume and pressure of detonation gas.

$$P = A\left(1 - \frac{\omega}{R_1 V}\right)e^{R_1 V} + B\left(1 - \frac{\omega}{R_2 V}\right)e^{R_2 V} + \frac{\omega E}{V}. \quad (6)$$

A and B are explosive parameters; R_1, R_2, and ω are performance parameters of explosives; E_0 is the internal energy of detonation gas; V is the relative volume of detonation gas.

Blasting pressure relief is to strengthen the range and damage degree of fracturing coal through deep-hole presplitting blasting, which is different from the conventional presplitting of joints cutting onsite. The larger hole spacing will lead to the existence of local complete coal blocks between holes, resulting in regional stress concentration. The calculated hole spacing of 2.4 m is more suitable for the initial penetration of cracks in the middle region. Therefore, it can be considered to shorten the spacing of blasting holes and strengthen the crack development between holes, so as to promote the pressure relief effect. The distribution characteristics of coal blasting-induced cracks under different hole spacing are shown in Figure 10.

For 2.4 m hole spacing, the cracks near blasting holes are relatively developed, while the main-wing cracks are

TABLE 9: **MAT_ADD_EROSION** parameters.

mxpres (MPa)	mnpres (MPa)	mxeps (10^{-2})	mneps (10^{-3})
19.20	-1.21	2.5	-5.6

Tips: *mxpres*: the maximum hydrostatic pressure is used for controlling the compression failure. *mnpres*: contrary to *mxpres*, it is used for controlling tensile failure with taking negative value. *mxeps*: the extreme value of principal strain is used for controlling compression failure. *mneps*: contrary to *mxeps*, the option is used for controlling tensile failure with as negative value.

connected to form the initial penetration of the cracks between blasting holes. The induced fracture would not form an effective pressure relief zone. When the hole spacing is 2.2 m, the crack tip of the fracturing zone produces secondary propagation under the action of explosive gas. Meanwhile, the fracture density is strengthened and developed intensively to form a rectangular fracturing zone with a minimum height of 0.29 m, which is conducive to the expansion of pressure relief zone. When the spacing is 2.0 m, the explosive gas wedging into the fracturing zone will further promote the development of circumferential wing cracks. A cross-connected stress releasing zone of main-wing cracks is formed between the blasting holes, and the minimum height (0.61 m) is approximately equal to the radius of fracturing zone. When the spacing is reduced to 1.5 m, the crack development degree near the blasting hole is similar to that of 2.0 m spacing, while the cracks are highly developed in the middle of holes. However, for the overall fracturing zone, the improvement effect of coal fracturing is not significant, but the drilling quantities increase significantly.
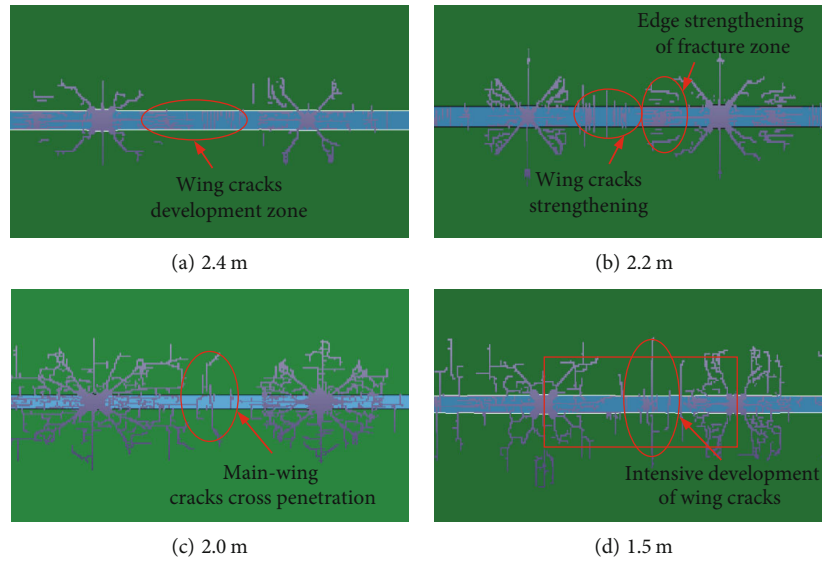
(a) 2.4 m

(b) 2.2 m

(c) 2.0 m

(d) 1.5 m

FIGURE 10: Distribution pattern of coal fracture under different blasting hole spacing.
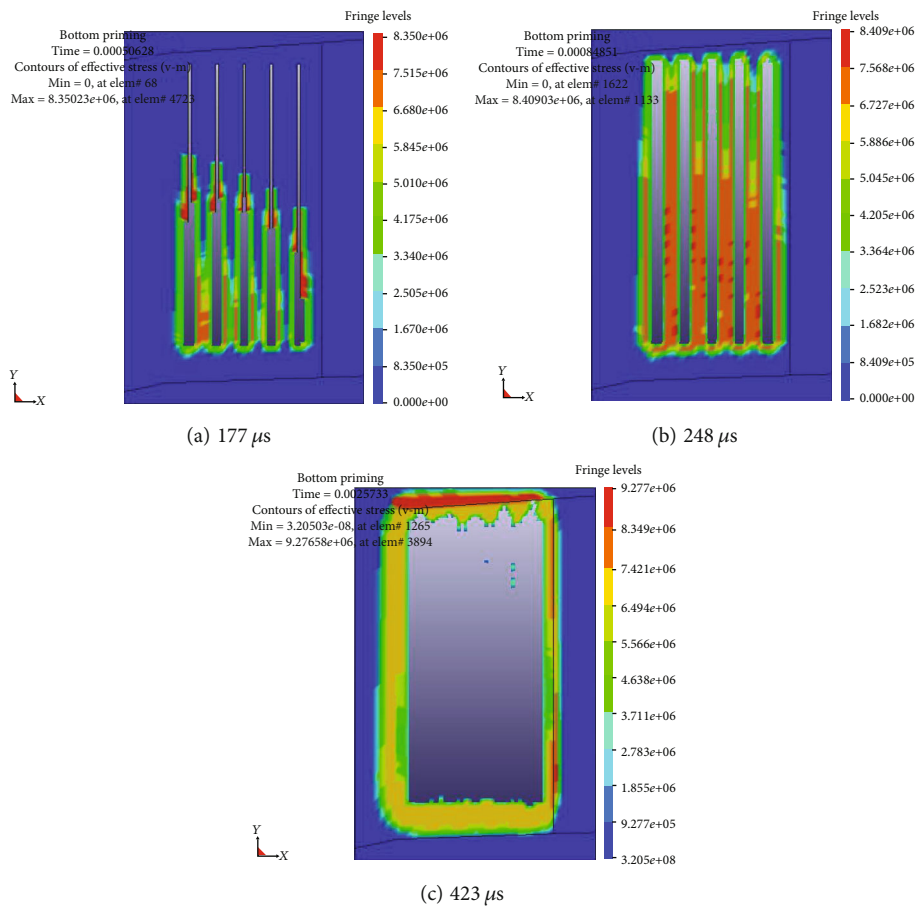

(a) 177 μs

(b) 248 μs

(c) 423 μs

FIGURE 11: Evolution process of equivalent stress in model section.

Based on the coal fracturing characteristics and cooperative pressure relief effect in the far-near field of blasting, considering that the crack development of raw coal onsite would reduce weakening efficiency of blasting, the spacing of blasting holes is set to be 2.0 m. The evolution profile of blasting crack at hole spacing of 2.0 m is shown in Figures 11 and 12.

Figure 11(a) shows the propagation process of stress wave along the aperture and axial direction after detonating the explosive in sequence; (b) is acting process of

(a) 96 μs

(b) 177 μs
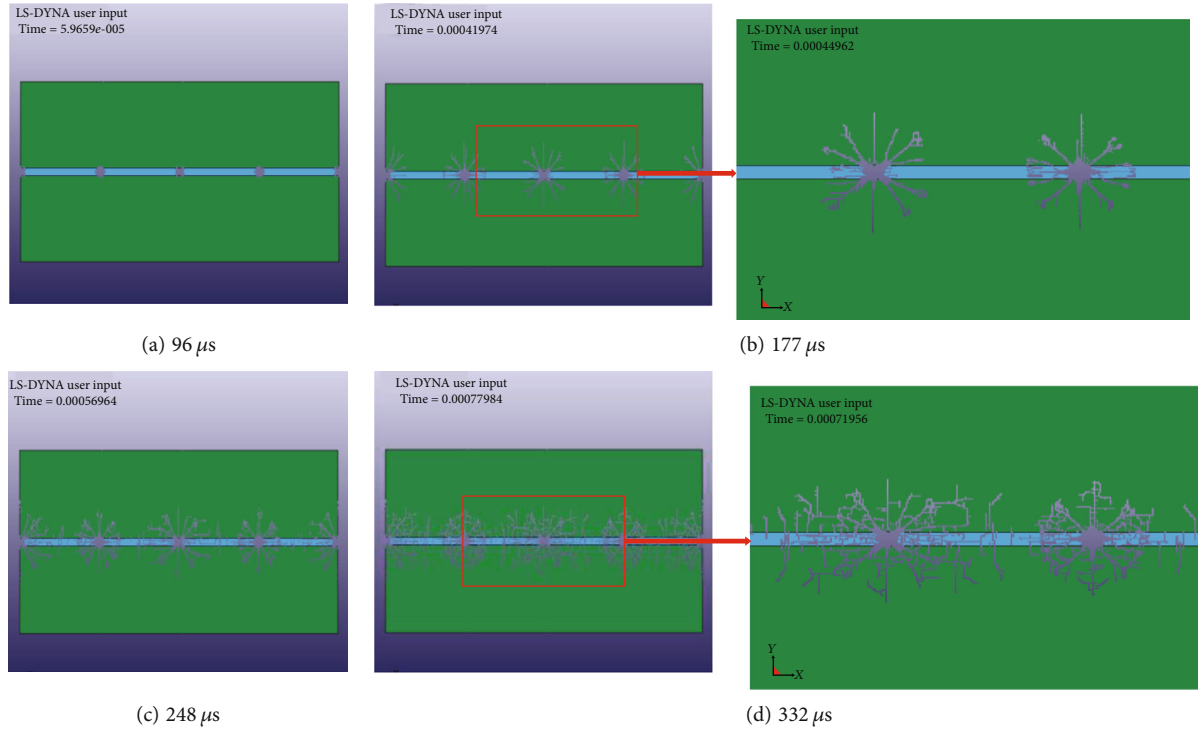
(c) 248 μs

(d) 332 μs

FIGURE 12: Evolution profile of blasting-induced crack.

equivalent stress; (c) is the stability result of the equivalent stress wave cracking on the section, showing that the coal between holes forms a crack field under the action of stress wave.

Figure 12(a) shows the crushing zone is formed in the vicinity of blasting hole at the initiation of 96 μs, and radius of development is 0.12 m; (b) is the stable developing radius of blasting cracks, which is 0.85 m; (c) is the stress wave cracking process in the connection line between holes center, which is the developing direction of the main cracks, linking up with each other at 248 μs; (d) is the intensive development process of the connected cracks between holes after the main crack connecting. Through detonation gas wedging into the wing crack cavities which connect with main cracks, the development of circumferential wing cracks is further enhanced, and the crisscross stress relief zoning of main and wing cracks with a minimum height of 0.61 m is formed between holes, providing larger space for the transfer and stress relief of coal. It shows the rationality of blasting holes space in stress relief.

4.3. Determination on Pressure Relief Effect with Deep-Hole Presplitting Blasting.
After blasting stress relief, the distribution characteristic of the abutment pressure under different in situ stress boundaries is shown in Figures 13 and 14, respectively.

With the increase of in situ stress, the transfer depth of stress peak decreases slightly (from 7.4 m to 5.6 m), and the stress peak and stress near roadsides increase in segments. In particular, when the in situ stress exceeds 38.4 MPa, the stress increases significantly. Under the condition of H region, the stress peak position is 14.8 m and the value is
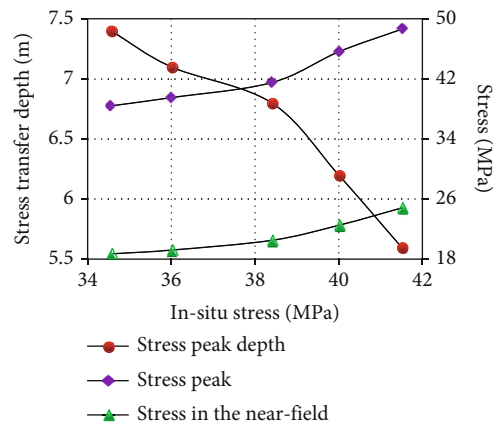

FIGURE 13: Variation of peak stress after blasting pressure relief under different in situ stress.

41.5 MPa. The peak position is 15.4 m, and the value is 38.4 MPa in M region, showing that the stress peak is well controlled. Meanwhile, the stress near the roadsides has been released and reduced to the safe range (18.7 MPa to 24.8 MPa). The above shows that the stress peak is obviously decreased and transferred to the deep, indicating the deep-hole blasting with the optimal parameters could effectively realize the pressure relief.

In general, the deep-hole blasting could effectively realize pressure relief under different in situ stress. When the coal fracturing degree of is low, especially under the influence of tectonic stress, the additional boreholes should be drilled between blast holes. The amount of pulverized coal drilled

(a) Model boundary stress 38.4 MPa (H region)

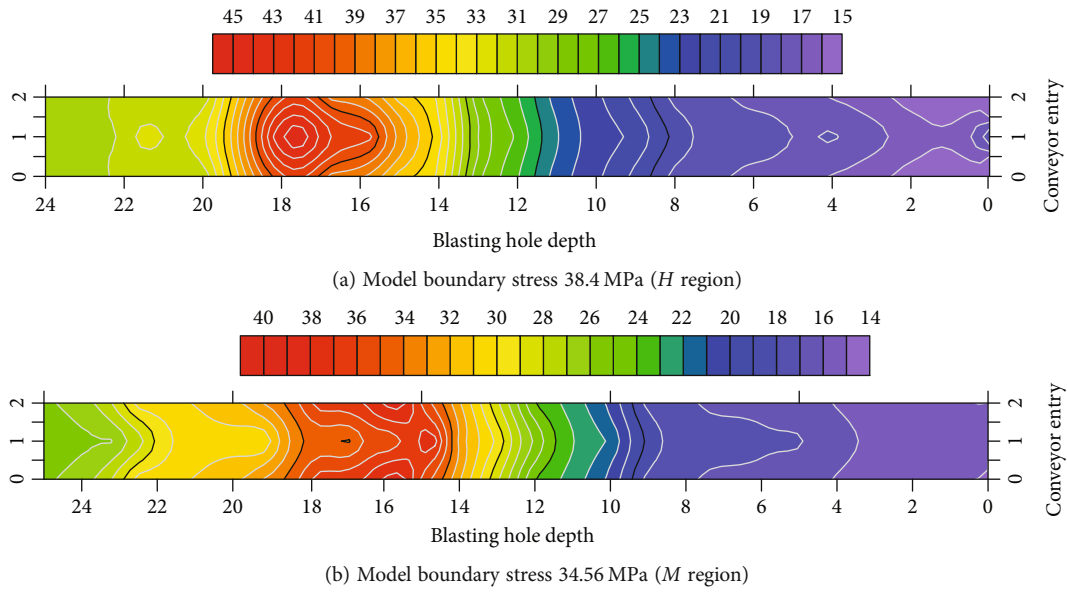(b) Model boundary stress 34.56 MPa (M region)

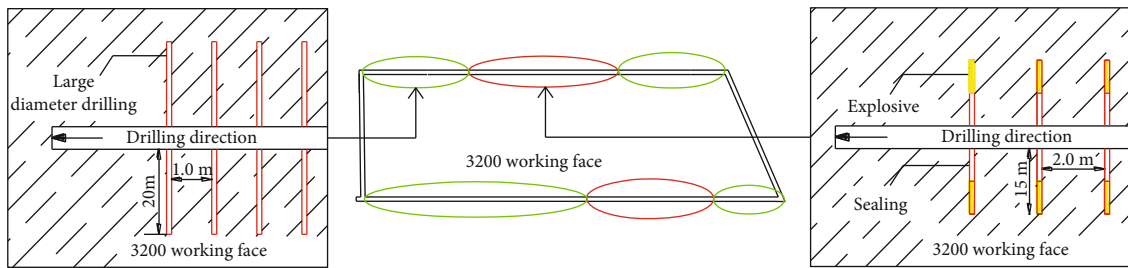Figure 14: Distribution of vertical stress after blasting stress relief.

Figure 15: Technological parameter of partition stress relief.

Table 10: Blasting hole parameters.

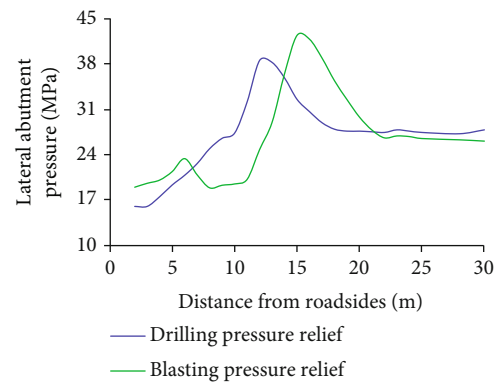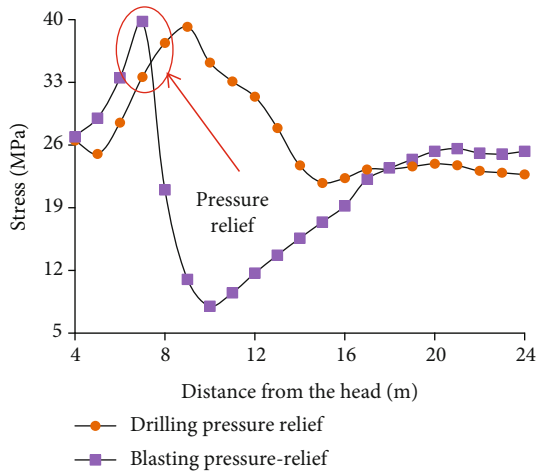| Elevation (°)	Height from floor (m)	Hole depth (m)	Charge length (m)	Charge weight (kg)	Hole spacing (m)	Drilling diameter (mm)	Charge diameter (mm)
6	0.7	15	6	12	2	66	48

Figure 16: Pressure curves of measure point before and after pressure relief in different pressure segments.

Figure 17: Displacement curve of roadway deformation after stress relief.

(a) Deformation of roadsides

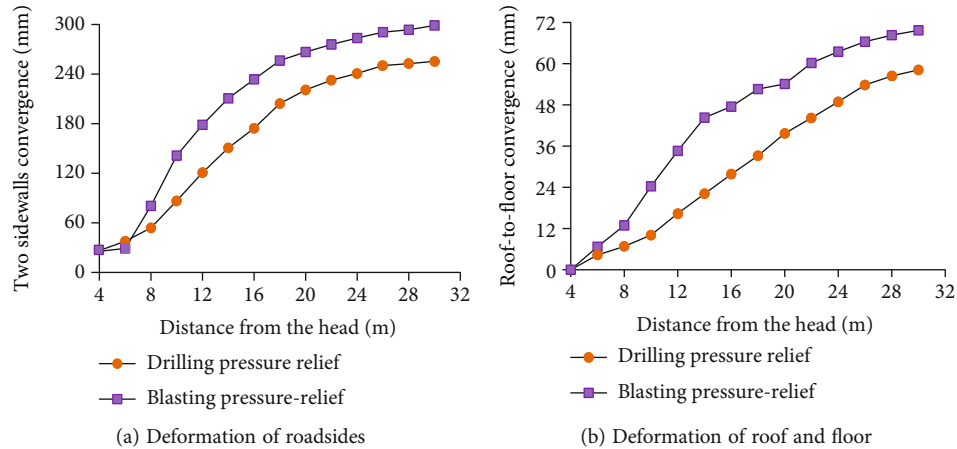(b) Deformation of roof and floor

FIGURE 18: Deformation characteristic of roadsides after pressure relief.

and the compensation space could be increased to realize the synergistic fracturing coal between blasting and drilling and further promote the pressure relief effect.

5. Effectiveness and Safety Evaluation of Pressure Relief on Site

5.1. Parameter Setting for Different Pressure Relief Methods

(1) Boreholes with 120 mm diameter and 20 m depth are drilled with hole spacing of 1.0 m in roadsides, as shown in Figure 15. It is located at 0.7 m from the floor and the maximum distance between boreholes and head-on should not exceed 10 m

(2) The elevation angle of boreholes is 5°, and the axial direction is parallel to dip angle of coal seam

(3) If the borehole cannot be drilled, the drilling can be continued by changing borehole position and circulating the excavation until the presetting depth is reached. If designing depth cannot be reached or the stress increases sharply due to effect of geological structure, the stress relief hole should be complementally drilled

For deep blasting, the borehole axial direction is parallel to the dip of coal seam. The borehole is reversely charged, and the detonating cord is bound firmly with the first explosive cartridge inserted into the bottom of the hole. The holes are connected in series with 3 m air column retained and sealed with 6.0 m expansive cement. The blasting parameters are shown in Table 10. The stress relief boreholes could be additionally drilled in the middle of the connecting line of holes center when the roadside pressure is larger.

5.2. Safety Validation of Field Pressure Relief Effect.

During the observation period, stress meters are placed in drilling boreholes 4.0 m from the head, in which the depth is 6.5 m. The initial injection pressure of stress meters is the same as initial stress of the coal. The stress near the roadsides and

lateral abutment pressure before and after pressure relief are shown in Figures 16 and 17.

Before borehole pressure relief, the abutment stress decreased slightly and then increased rapidly during excavation. The stress increased slowly after drilling boreholes and reached the maximum value of 38.5 MPa at the position lagging behind head-on at 9.0 m, meaning the coal was in a state of stress concentration with a high risk of rockbursts. After borehole stress relief, the stress decreased slowly and tended to be stable (23.2 MPa) when lagging behind the head-on at 14.5 m, during which the maximum stress decreased by 39.7%. Before the blasting stress relief, the abutment stress increased rapidly and reached the maximum value of 39.8 MPa when lagging behind the head-on at 7 m. The stress rapidly dropped to the minimum value of 8.3 MPa after blasting when lagging behind the head-on at 10.2 m. Then, it recovered slowly and tended to be stable (25.2 MPa) when lagging behind the head-on at 18.2 m, during which the decreasing rate is 36.7%. The above shows that the coal stress near the roadsides is in the controllable safety range after pressure relief.

For the borehole pressure relief, the stress near the roadsides was low (16.2 MPa) after the borehole pressure relief. With the increase of the roadside depth, the stress reached the peak value of 38.5 MPa at 12.2 m. After pressure relief with deep-hole blasting, the stress of roadsides was low (18.8 MPa), but there was a small range of stress concentration at the sealing section of the blasting hole. However, within the weakening range of blasting, the stress reached a minimum (18.9 MPa within the range of 8.0-12.0 m), and then, the lateral abutment pressure increased rapidly until it reached the peak of 42.4 MPa at 14.7 m.

The stress transfer to the deep is more significant than that before pressure relief, and the stress near the roadsides is in a lower stress state. It is shown that large-diameter borehole and blasting stress relief could effectively change stress distribution in different partitions, and the stress decrease is obvious. Thus, it can be concluded that the pressure relief effect is remarkable.

The deformation of roadway after pressure relief is shown in Figure 18.

After stress relief, the roadway is significantly deformed. Under the condition of drilling stress relief, the displacement of the roadside convergence is increasing from 26.5 mm (before) to 255.4 mm (after), with the deformation of roof to floor from 4.3 mm to 58.2 mm. Under the condition of blast stress relief, the displacement of the roadside convergence is increasing from 25.6 mm (before) to 298.8 mm (after), with the deformation of roof to floor from 6.7 mm to 69.7 mm. The displacement is less than the maximum allowable value of roadway deformation, indicating the roadway displacement produced by stress relief is under control.

6. Conclusions

(1) Based on the multifactor evaluation on dynamic risk, it is proposed that the partition division of risk degree is 28.8 MPa, 34.56 MPa, and 38.4 MPa. According to the multifactor influence characteristics of stress field, the dangerous zones of roadside stress are divided, and the safe pressure relief strategy is put forward. The rationality and feasibility of pressure relief measures are proved

(2) Under the condition of drilling stress relief, the orthogonal simulation test reveals that the diameter, depth, and hole spacing determine the stress peak location of roadsides and the diameter and hole spacing determine the stress distribution in the near field. Meanwhile, the deformation degree mainly depends on the diameter and hole spacing. Therefore, the optimal combination of parameters is obtained with $A4B4C1D2$ (i.e., 120 mm hole diameter, 20 m hole depth, 1.0 m hole spacing, and 5° elevation angle) through analysis of significance level and contribution rate. However, the optimal parameter of boreholes for stress relief could only achieve a significant relief effect at the partition below the medium danger (less than 34.56 MPa)

(3) For the stress partition above the medium danger, the decoupling factor and hole spacing of blasting are determined to be 1.3 and 2.0 m, respectively. Through simulation analysis on the fracturing process and the intensive morphological development of main-wing cracks, it can be obtained that a cross-connected stress relief zone with a minimum height of 0.61 m is formed between holes. After blasting stress relief, the stress peak depth is 14.8 m (H region) and 15.4 m (M region), and the peak value is 41.5 MPa (H region) and 38.4 MPa (M region). The stress peak is obviously decreased and transferred to the deep, indicating the deep-hole blasting technology could effectively realize the pressure relief

(4) Verifying the stress relief effect of boreholes and deep-hole blasting via observation of stress meters and deformation measuring points, the decreasing rate of the stress is 39.7% and 36.7%, respectively, and the depth of stress transfer is 12.2 m and 14.7 m. Meanwhile, the maximum displacement at the convergence of roadsides is 255.4 mm and 298.8 mm, respectively. The stress near roadsides and displacement is under control overall, proving that pressure relief effect is shown to be remarkably helpful

Data Availability

The data used to support the findings of this study are available from the corresponding author upon request.

Conflicts of Interest

The authors declare that there is no conflict of interest regarding the publication of this paper.

Acknowledgments

References

[1] J. M. Alcott, P. K. Kaiser, and B. P. Simser, "Use of microseismic source parameters for rockburst hazard assessment," *Pure and Applied Geophysics*, vol. 153, no. 1, pp. 41–65, 1998.

[2] V. A. Eremenko, L. N. Gakhova, and N. Semenyakin, "Formation of higher stress zones and clusters of seismic events in deep mining in Tashtagol," *Journal of Mining Science*, vol. 48, no. 2, pp. 269–275, 2012.

[3] L. S. Jiang, P. Wang, and P. P. Zhang, "Numerical analysis of the effects induced by normal faults and dip angles on rock bursts," *Comptes Rendus Mécanique*, vol. 345, no. 10, pp. 690–705, 2017.

[4] S. Zhu, F. Jiang, and J. Liu, "Research on mechanism of rock burst and large deformation coordination controlling in thick coal seam of deep shaft," *Chinese Journal of Rock Mechanics and Engineering*, vol. 34, pp. 4262–4268, 2015.

[5] Z. L. Wang, Y. C. Li, and R. F. Shen, "Numerical simulation of tensile damage and blast crater in brittle rock due to underground explosion," *International Journal of Rock Mechanics and Mining Sciences*, vol. 44, no. 5, pp. 730–738, 2007.

[6] D. Z. Song, E. Y. Wang, J. K. Xu, X. Liu, R. Shen, and W. Xu, "Numerical simulation of pressure relief in hard coal seam by water jet cutting," *Geomechanics and Engineering*, vol. 8, no. 4, pp. 495–510, 2015.

[7] J. W. Liu, C. Y. Liu, Q. L. Yao, and G. Y. Si, "The position of hydraulic fracturing to initiate vertical fractures in hard hanging roof for stress relief," *International Journal of Rock Mechanics and Mining Sciences*, vol. 132, article 104328, 2020.

[8] J. W. Liu, C. Y. Liu, and X. H. Li, "Determination of fracture location of double-sided directional fracturing pressure relief for hard roof of large upper goaf-side coal pillars," *Energy Exploration & Exploitation*, vol. 38, no. 1, pp. 111–136, 2020.

[9] X. Liu, G. Xu, C. Zhang et al., "Time effect of water injection on the mechanical properties of coal and its application in rockburst prevention in mining," *Energies*, vol. 10, no. 11, article 1783, 2017.

[10] M. Wang, X. Y. Wang, and T. Q. Xiao, "Borehole destressing mechanism and determination method of its key parameters in deep roadway," *Journal of China Coal Society*, vol. 42, no. 5, pp. 1138–1145, 2017.

[11] J. H. Liu, F. X. Jiang, S. T. Zhu, H. Li, and Q. J. Zhu, "Rock burst model of typical coal seam under thick alluvium," *Journal of China Coal Society*, vol. 45, no. 5, pp. 1753–1763, 2020.

[12] E. B. Yi, Z. L. Mu, L. M. Dou, J. G. Ju, L. Xie, and D. L. Xu, "Study on comparison and analysis of pressure releasing effect of boreholes in soft and hard seam," *Coal Science and Technology*, vol. 39, no. 6, pp. 1–5, 2011.

[13] S. C. Zhang, Y. Y. Li, B. T. Shen, X. Z. Sun, and L. Q. Gao, "Effective evaluation of pressure relief drilling for reducing rock bursts and its application in underground coal mines," *International Journal of Rock Mechanics and Mining Sciences*, vol. 114, pp. 7–16, 2019.

[14] Z. Q. Yang, L. M. Dou, C. Liu, M. Xu, Z. Lei, and Y. Yao, "Application of high-pressure water jet technology and the theory of rock burst control in roadway," *International Journal of Mining Science and Technology*, vol. 26, no. 5, pp. 929–935, 2016.

[15] P. Konicek, K. Soucek, L. Stas, and R. Singh, "Long-hole destress blasting for rockburst control during deep underground coal mining," *International Journal of Rock Mechanics and Mining Sciences*, vol. 61, pp. 141–153, 2013.

[16] M. R. Saharan and H. Mitri, "Destress blasting as a mines safety tool: some fundamental challenges for successful applications," *Procedia Engineering*, vol. 26, pp. 37–47, 2011.

[17] Z. G. Liu, A. Y. Cao, G. A. Zhu, and C. B. Wang, "Numerical simulation and engineering practice for optimal parameters of deep-hole blasting in sidewalls of roadway," *Arabian Journal for Science and Engineering*, vol. 42, no. 9, pp. 3809–3818, 2017.

[18] Y. H. Cheng, F. X. Jiang, Z. F. Hu, and J. K. Lin, "Prevention and control of coal burst on gob-side entry in deep coal seam with fully mechanized sublevel caving mining," *Chinese Journal of Rock Mechanics and Engineering*, vol. 35, pp. 3000–3007, 2016.

[19] J. Wen, H. Li, F. Jiang, Z. Yu, H. Ma, and X. Yang, "Rock burst risk evaluation based on equivalent surrounding rock strength," *International Journal of Mining Science and Technology*, vol. 29, no. 4, pp. 571–576, 2019.

[20] A. Mazaira and P. Konicek, "Intense rockburst impacts in deep underground construction and their prevention," *Canadian Geotechnical Journal*, vol. 52, no. 10, pp. 1426–1439, 2015.

[21] L. Z. Ye and X. J. Zhu, "Analysis of cavitation orthogonal experiments in power ultrasonic honing," *Advances in Mechanical Engineering*, vol. 9, 168781401771210 pages, 2017.

[22] B. Zakrisson, B. Wikman, and H. K. Häggblad, "Numerical simulations of blast loads and structural deformation from near- field explosions in air," *International Journal of Impact Engineering*, vol. 38, no. 7, pp. 597–612, 2011.

[23] C. Y. Liu, J. X. Yang, and B. Yu, "Rock-breaking mechanism and experimental analysis of confined blasting of borehole surrounding rock," *International Journal of Mining Science and Technology*, vol. 27, no. 5, pp. 795–801, 2017.

[24] Livermore Software Technology Corporation, *LS-DYNA Keyword User's Manual*, LSTC, USA Livermore California, 2003.